Received: 10 November 2021 | Revised: 4 March 2022 | Accepted: 8 March 2022

DOI: 10.1002/mp.15637

RESEARCH ARTICLE

MEDICAL PHYSICS

A high-resolution dose calculation engine for X-ray microbeams radiation therapy

Sarvenaz Keshmiri[1] | **Sylvan Brocard**[1] | **Raphaël Serduc**[1,2] | **Jean-François Adam**[1,2]

[1]Université Grenoble-Alpes, UGA/INSERM UA7 STROBE, 2280 rue de la Piscine, Saint-Martin d'Hères 38400, France

[2]Centre Hospitalier Universitaire Grenoble-Alpes, CS10217, Grenoble 38043, France

Correspondence
Jean-François ADAM, Univ. Grenoble Alpes, INSERM, UA07 STROBE, Grenoble 38000, France.
Email: jean-francois.adam@univ-grenoble-alpes.fr

Funding information
LabEx PRIMES, Grant/Award Number: ANR-11-LABX-0063/ANR-1-IDEX-0007

Abstract

Background: Microbeam radiation therapy (MRT) is a treatment modality based on spatial fractionation of synchrotron generated X-rays into parallel, high dose, microbeams of a few microns width. MRT is still an underdevelopment radiosurgery technique for which, promising preclinical results on brain tumors and epilepsy encourages its clinical transfer.

Purpose: A safe clinical transfer of MRT needs a specific treatment planning system (TPS) that provides accurate dose calculations in human patients, taking into account the MRT beam's properties (high-dose gradients, spatial fractionation, polarization effects). So far, the most advanced MRT TPS, based on a hybrid dose calculation algorithm, is limited to a macroscopic rendering of the dose and does not account for the complex dose distribution inherent to MRT if delivered as conformal irradiations with multiple incidences. For overcoming these limitations, a multi-scale full Monte-Carlo calculation engine called penMRT has been developed and benchmarked against two general-purpose Monte Carlo (MC) codes: penmain based on PENELOPE and Gate based on Geant4.

Methods: PenMRT, is based on the PENELOPE (2018) MC code, modified to take into account the voxelized geometry of the patients (computed tomography [CT]-scans) and is offering an adaptive micrometric dose calculation grid independent of the CT size, location, and orientation. The implementation of the dynamic memory allocation in penMRT, makes the simulations feasible within a huge number of dose scoring bins. The possibility of using a source replication approach to simulate arrays of microbeams, and the parallelization using OpenMPI have been added to penMRT in order to increase the calculation speed for clinical usages. This engine can be implemented in a TPS as a dose calculation core.

Results: The performance tests highlight the reliability of penMRT to be used for complex irradiation conditions in MRT. The benchmarking against a standard PENELOPE code did not show any significant difference for calculations in centimetric beams, for a single microbeam and for a microbeam array. The comparisons between penMRT and Gate as an independent MC code did not show any difference in the beam paths, whereas, in valley regions, relative differences between the two codes rank from 1% to 7.5% which are probably due to the differences in physics lists that are used in these two codes. The reliability of the source replication approach has also been tested and validated with an underestimation of no more than 0.6% in low-dose areas.

Conclusions: Good agreements (a relative difference between 0% and 8%) were found when comparing calculated peak to valley dose ratio values using penMRT, for irradiations with a full microbeam array, with calculated values in the literature. The high-resolution calculated dose maps obtained with penMRT are used to extract differential and cumulative dose–volume histograms (DVHs) and analyze treatment plans with much finer metrics regarding the irradiation complexity. To our knowledge, these are the first high-resolution dose maps and associated DVHs ever obtained for cross-fired microbeams irradiation, which is bringing a significant added value to the field of treatment planning in spatially fractionated radiation therapy.

KEYWORDS
dose calculation engine, medium energy X-rays, microbeam radiation therapy, micrometric dose calculation grids, Monte Carlo method, synchrotron radiation

1 | INTRODUCTION

The outcome of radiation therapy in terms of efficacy and toxicity relies on a compromise made between maximizing the deposited radiation dose in the tumoral area and minimizing the damage to healthy tissues by keeping the radiation dose delivered to these organs as low as possible.[1] Microbeam radiation therapy (MRT) is a disruptive radiotherapy approach aiming at widening the therapeutic window by combining the spatial fractionation of synchrotron generated X-rays into an array of intense parallel microbeams (25–50-μm wide beams replicated with a pitch of 200–400 μm) with an irradiation performed at high dose rate to benefit from the improved healthy tissue tolerance due to the FLASH effect.[2–4] MRT pushes the concept of dose–volume effect to its theoretical limits with high doses delivered in the microbeam paths (peak doses), whereas low-dose areas are found in-between these tracks (valley doses). Several preclinical studies have demonstrated the potential of MRT for improving tumor control with reduced side effects.[5–8]

The quality of MRT relies on several physical parameters, mainly the X-ray energy and the dose rate. The optimal energy for this treatment varies from 100 to 300 keV as shown by simulations[9] and confirmed experimentally at the Australian Synchrotron.[10] Low- to medium energy photons are required despite their lower penetration ability as they offer sharp penumbras and short lateral electronic equilibrium distances, thus keeping the dose between the microbeams as low as possible. Furthermore, the high dose rate is necessary to guarantee short irradiation times and minimize the blurring effect caused by the organ motions.[11] The third-generation synchrotron sources provide the high-flux X-ray beams with the required spectral properties to be adequately used for MRT.[12]

After two decades of preclinical studies, the clinical transfer of MRT in oncology and epilepsy management has started in the frame of large animal studies. Several challenging medical physics issues have to be managed to expand the concept of MRT to human patients treatments.[13] Accurate experimental dosimetry and online monitoring tools are being developed,[10,14] together with state-of-the-art dose calculation engines,[15] beam and patient positioning[16] and patient-specific quality assurance.[17]

In the past decade, numerous studies aimed at validating the dose calculation engines developed for microbeam radiotherapy. The majority of these calculation engines are based on Monte Carlo (MC) methods, considering the extremely small beam sizes and the properties of synchrotron X-rays. These studies were conducted using various MC codes, hence with different physical models: INHOM (EGS4),[18] PENELOPE,[19–23] Geant3 PSI-version,[24] Geant4,[25–28] EGS4,[29–31] EGS5,[32] MCNPX[33] and EGSnrc.[34] A comparative study by De Felici et al., summarized the effect of different MC codes on in-field and out-of-field doses[34]: in field doses were found similar amongst all the codes that have been investigated, whereas Geant4 gave significantly different out of field dose values.

The first attempt to create an MRT treatment planning system (TPS) being able to use an adequate dose calculation engine on dosimetry computed tomography (CT) data was performed by Martínez-Rovira et al.,[22] at the European Synchrotron Radiation Facility (ESRF) medical beamline (ID17). This full MC dose calculation algorithm based on PENELOPE/penEasy was modeling the whole ESRF medical beamline components. However, it could only be used for unidirectional treatment and non-conformal irradiation fields. The implementation of this method in a full TPS has been proposed, providing 3D conformal MRT could be performed in clinically compatible calculation times.

Several alternative methods aiming at drastically reducing the dose calculation time were proposed in order to reach a clinically compatible MRT TPS. A kernel-based method was developed by Debus et al.[35] This remarkably fast algorithm is based on analytical

TABLE 1 A summary of the existing dose calculation engines for MRT

Algorithm name	Developer and year	Calculation method	Advantages	Limitations	Coupled to a TPS
PenEasy	Martínez-Rovira et al. (2012)[22]	PENELOPE MC code	The first precise micrometric dose calculation engine for MRT	1. Time consuming 2. Limited to unidirectional treatment 3. Only for non-conformal fields	No
Kernel based	Debus et al. (2017)[35]	Pre-calculated kernels for photons and electrons	Fast calculation	1. Lack of accuracy in valley doses and heterogeneous medium 2. Not able to consider the photon polarization	Yes VIRTUOS
Ray-tracing	Poole et al. (2017)[36]	Pre-calculated PVDRs	Fast calculation	Lack of precision	Yes Eclipse
Hybrid	Donzelli et al. (2018)[37]	Mixed method: 1. Photons transport from Geant4 MC code 2. Electron transport from kernel-based method	1. Fast calculation 2. Dose calculation in multidirectional treatment 3. Taking into account the conformal beams	1. Limited to the macroscopic rendering of separated peak and valley doses	Yes Eclipse[38]

Abbreviations: MRT, microbeam radiation therapy; PVDR, peak to valley dose ratio; TPS, treatment planning system.

pre-calculated kernels for scattered electrons and photons. However, its accuracy is significantly lower at interfaces, valley areas and beam entrances and it is not able to take into account the photon polarization. Another simple but fast dose calculation algorithm with limited precision was developed by Poole et al.,[36] based on pre-calculated peak to valley doses ratios (PVDRs) and ray-tracing. More recently, a hybrid algorithm has been developed by Donzelli et al.,[37] at the ESRF-ID17. In this hybrid algorithm, the primary and scattered photon's energy transfer is calculated using Geant4 MC code. Afterward, the convolution of pre-calculated electrons dose kernels with the MRT fluence pattern creates peak doses. Valley doses are calculated from scattered photon interactions and added to the peak doses. According to the authors, this method is 600 times faster than a full straightforward MC method. The cost of this rapidity is being limited to the macroscopic rendering of separated peak and valley dose maps (see Figure 6 in Ocadiz et al.[17]). With the perspective of being used in MRT pre-clinical and clinical trials, some of these algorithms were successfully implemented in commercial TPSs. The kernel-based method[35] has been coupled to VIRTUOS (A program for VIRTUal radiOtherapy Simulation and verification),[15] the ray-tracing method has been included in Eclipse TPS (Varian Medical Systems, Palo Alto, CA)[36] and recently, the hybrid algorithm is used as a calculation core for MRT in the research version of the Eclipse TPS.[38] A summary of described existing algorithms is given in Table 1.

Until now, none of the developed dosimetry tools combine all the requirements for clinical use in an MRT dedicated TPS: precision, time efficiency, and spatial resolution. In particular, as MRT leads to high dose gradients replicated at a micrometric scale inside the irradiation field, it is necessary to provide a precise micrometric dose calculation engine in order to understand the underlying radiobiological mechanisms of MRT, when being used as multidirectional treatments.[8]

In this study, we developed a full high-resolution MC dose calculation engine based on PENELOPE which is capable of taking into account the 3D conformal MRT fields, to be used as a calculation core in a clinical MRT-TPS. This calculation engine aims at being reliable, fast enough to ensure dose calculation in a clinical context. It should also allow the display of high-resolution (5 μm) dose maps and high-resolution dose metrics for MRT.

2 | MATERIALS AND METHODS

2.1 | Monte Carlo simulation code: PENELOPE

Since MRT deals with electron and photon energy lower than conventional radiotherapy on micrometric scale, the choice of an adequate MC code has a crucial role. The choice of MC code depends on its simulation strategy class and implemented physical model. Among all the available MC codes, based on required characteristics,

PENELOPE[39] was chosen for this work and upcoming developments. PENELOPE is a well-known MC code in the medical physics domain[40,41] for simulating the photons and electrons/positrons transport within a wide energy range from 50 eV to 1 GeV in a large number of materials. The choice of PENELOPE is driven by the fact that PENELOPE uses a mixed simulation strategy, allowing detailed or condensed history calculations for the electrons/positrons transport, based on the compromises that should be made between the calculation time and the level of accuracy. Besides, its random-hinge algorithm provides a detailed description of low-energy electron transport which is important for valley dose calculation. Compton differential cross-section (CDCS) is also a critical subject, as it can influence the absorbed dose in narrow passages of radiation (peaks), interfaces, entrance doses[42] and the absorbed dose due to scattering (valley). In order to calculate CDCS, PENELOPE uses the relativistic impulse approximation rather than Klein-Nishina rough approximation or Waller–Hartree formalism.[39] This approximation takes into account Doppler broadening and binding effects and it shows a good agreement with experimental data, especially at low energies.[43,44] Thanks to these features, PENELOPE has been used as a simulation tool for stereotactic radiosurgery[45] in which high precision is mandatory.[46] Furthermore, the efficiency of this code in microdosimetry and nanodosimetry has been proven.[47,48] Based on the aforementioned characteristics and also a precise model for polarized photons in PENELOPE (which is the case of synchrotron-produced X-rays), this code can meet all specific requirements for MRT. In this work, we developed a structured general-purpose main MC parallelized dose calculation engine for MRT, based on the latest version of PENELOPE (2018), but modified for accounting for MRT requirements.

2.2 | PenMRT: PENELOPE for MRT

The main program developed for MRT is called penMRT (PENELOPE for MRT). The general-purpose main program (penmain) has been modified for being able to perform dose calculations in adaptive grids that are not linked to the CT scan voxel size, orientation and location. Penmain has also been modified to read voxelized geometries and quadric geometries at the same time. These modifications have been inspired by the work performed by Sempau et al. for penEasy.[41] A systematic parallelization using OpenMPI has also been implemented in penMRT. The comparison between block diagrams of penmain and penMRT, shown in Figure 1, highlights the fundamental features of penMRT.

Geometric features of penMRT. PenMRT initializes the geometry and tracks particles in quadric geometries in the same ways as penmain (Figure 1a). However, if a voxelized geometry has been declared (based on a keyword "CT" in the initialization file), it activates the particle tracking specific to voxelized geometry (top box, Figure 1b). Thus, the voxelized geometry subroutine works alongside with quadric geometry subroutine to handle together voxelized structures and quadric structures in the same simulations without requiring temporary phase-space files (PSFs). The location tracking subroutine (LOCATE) has been modified so that if penMRT detects a particle entering a voxelized geometry, it calls its homolog in voxelized geometry subroutine (CTLOC, bottom box, Figure 1b).

In order to allow simulations for beams at various angles, it is required to rotate and translate each primary particle together with the dose calculation grid by using a specific subroutine (PCTSET). When the particles exit the CT structure, these modifications in trajectory and position are reversed by activating another subroutine (PCTUNSET). The advantage of this method is that there is no longer a need for an external program to rotate the voxelized geometry such as in PenEasy or PenCT.[22,41,49] Everything is now controlled in the main script, which reduces the risk of potential errors. The subroutines are responsible for determining the position and direction of particles after each event were kept intact. However, the JUMP subroutine is modified to provide a distance to travel in CT structure as well as in quadric geometry.

Radiation source replication in penMRT. In MRT, the radiation source consists of an array of microbeams separated by the desired center-to-center distance. This array is produced by using a so-called multislit collimator (MSC).[50] Planning in MRT also requires simulations of broad beams as the irradiation parameters are given in a reference non fractionated field. To that respect, penMRT is able to account for both source geometries (Figure 2). The calculation time could be prohibitively long if the simulation includes the multislit because the amount of particles that are lost is higher than 85% of the primary particles generated from the source. Thus, to have an acceptable uncertainty in dose calculations, without increasing the calculation time, it has been decided to implement a source replication feature in penMRT (Figure 2b). To this respect, a single microbeam source is modeled to the appropriate width and height. Each primary photon is then allocated to a given microbeam using a lateral translation ensuring random distribution in all the microbeams from the array. This feature is interesting because it can enable the modeling of non-homogeneous intensity profiles (roll-off effect) by applying the distribution profile to the random translation.

Multiscale adaptive dose grids in penMRT. Covering the whole patient data with a micrometric dose calculation grid demands a huge computational capacity and is not feasible in practice. Besides, a considerable fraction of the geometry receives a negligible dose. A function

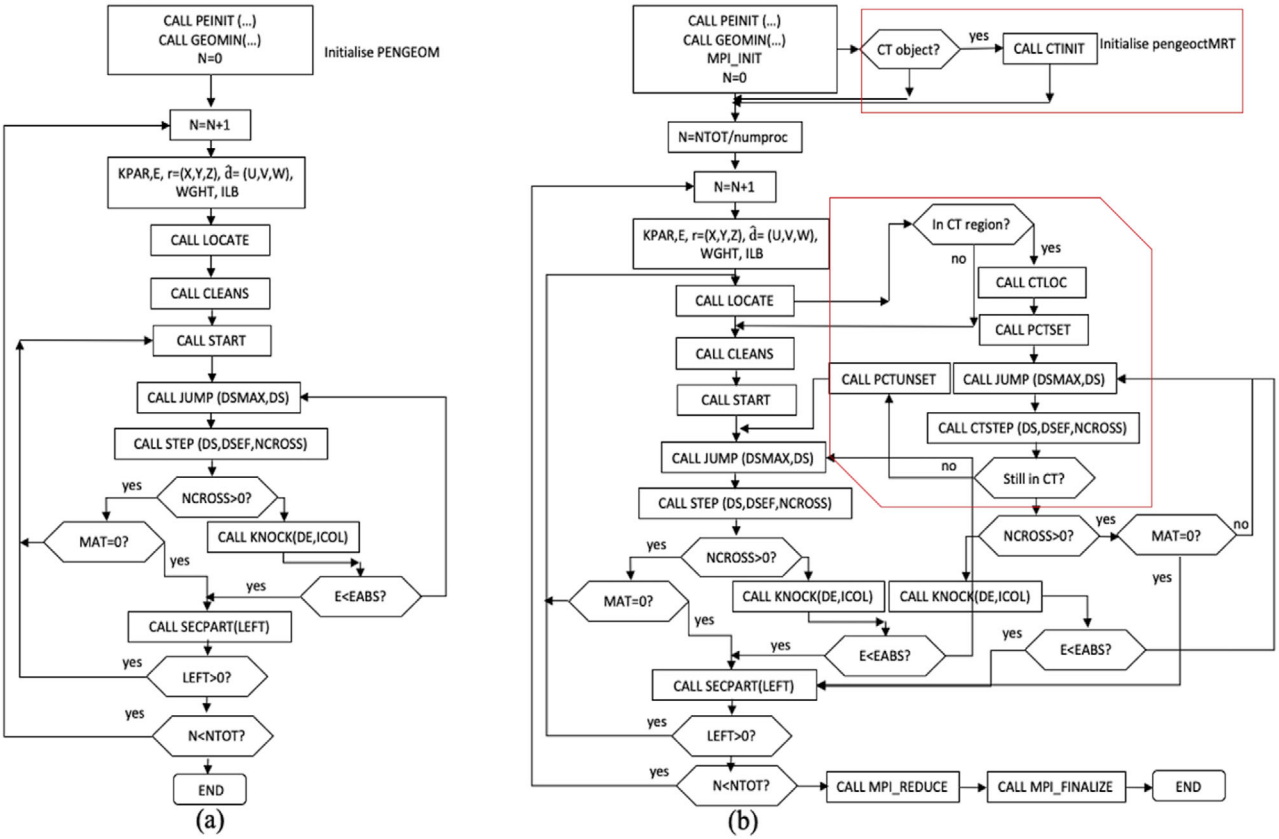

FIGURE 1 (a) Block-diagram of penmain released by Salvat et al.[39] (b) Block-diagram of penMRT highlighting voxelized geometry processing along with quadric geometry and parallelization

has been implemented in penMRT that establishes a multiscale dose calculation grid and, with the possibility for the user to define the resolution of the dose calculation grids according to the area of interest. Typically, high-resolution dose calculation grids are $0.005 \times 1 \times 1$ mm^3, where the 0.005 mm is perpendicular to the incident beam axis in order to measure peaks, valleys and the transition of peak to valley zones. The medium and low-resolution dose calculation grids are $1 \times 1 \times 1$ and $10 \times 10 \times 1$ mm^3, respectively. It is desirable to cover the beam passage with a high-resolution grid, and the user is free to choose the grid resolution and location, based on their specific needs. An example of dose calculation grids configurations is shown in Figure 3. With this adaptive dose calculation grid, penMRT is able to calculate dose maps at a micrometric and millimetric scale at the same time, to give a macroscopic vision of the entire zone irradiated by microbeam arrays.

PENELOPE simulations parameters for penMRT. In penMRT, the absorption energies (EABS), as well as the cutoff energies for hard inelastic events (WCC) and hard bremsstrahlung events (WCR) have been set to 10 keV for electrons and 1 keV for the photons.[39] This ensures a mean free path of photons (2.51 μm in water at 1 keV) and a range of secondary electrons (2.45 μm in water at 10 keV) significantly smaller than the size of the dose calculation grids. Another important parameter that has an impact on charged particles' transport is the maximum average angular deflection in multiple-scattering (C1) and the maximum average fractional energy loss along the step (C2) which are at the basis of the mixed approach of PENELOPE. The minimum value of C1 and C2 (C1 = C2 = 0) results in a detailed time-consuming simulation and on the contrary, the maximum values of C1 and C2 (C1 = C2 = 0.2) accelerate simulations to the cost of a reduced precision in small dose grids.[39,46] A detailed study was done by Martínez-Rovira et al.[22] to quantify the effect of these parameters on calculation speed and the precision. In our study, three values of C1 and C2 values of 0.01, 0.05, and 0.1 were tested in order to find an optimal value for subsequent use. Synchrotron-generated X-rays are linearly polarized in the horizontal plane.[22] As photon polarization affects the calculated dose away from the beam center,[29] in performance tests, polarization is taken into account by setting the Stoke parameter P_3 to -1. Stoke parameter P_3 represents linear polarization and the value -1 meaning maximum polarization in a horizontal plane.

Improved computational capacity and parallelization of penMRT. Originally, in PENELOPE, the memory allocation for dose calculation grids is a static allocation. This limits the computational capacity and the dose

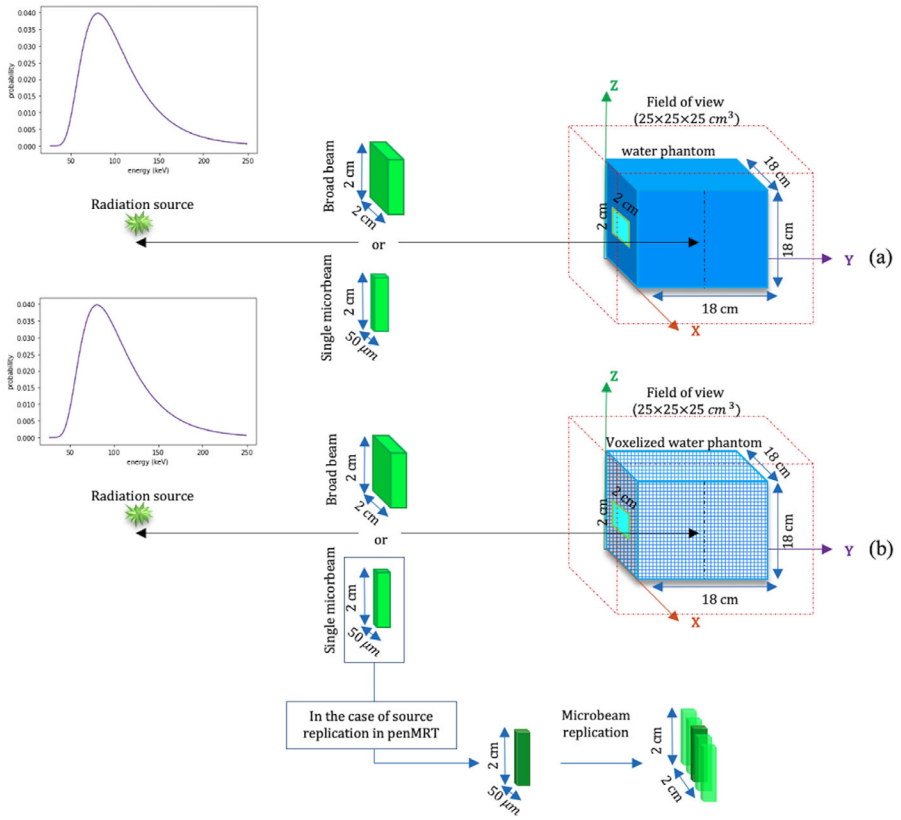

FIGURE 2 Geometric characteristics of penMRT. (a) A quadric geometry (b) or/and a voxelized geometry can be taken into account. A source replication option is added to penMRT in order to discard the need to model the multislit collimator. A typical synchrotron-generated X-ray filtered spectrum, as used in small animals studies, is represented on the left

calculation is confined to a specific number of bins (typically 512 × 512 × 512). We implemented the dynamic memory allocation in penMRT instead of the static one, by using the Fortran 90 related features. The dose calculation capacity has been significantly increased with the dynamic memory allocation, allowing a continuous simulation of some hundreds of millions of dose bins and the production of simulation output files which are updated at the user-specified time intervals. The memory capacity is a limiting factor. A typical simulation for a 2 × 2 cm^2 MRT field with more than 10^7 micrometric dose scoring bins needs 7 GB of memory per thread.

A "Single Program Multiple Data" (SPMD) scheme using OpenMPI[51] has been implemented in penMRT, to be able to run the simulation on a cluster of CPUs, by using various sets of seeds in the random number generator used by PENELOPE, without recycling multiple times the results generated from the same seed and introducing unwanted bias.

2.3 | Post-processing in penMRT

A set of post-processing scripts necessary for analyzing the results has been developed for penMRT using Python 3.9 in order to visualize and analyze the dose maps. In the case of multi-directional treatments, each beam is simulated separately (see Figure 3a and b). The dose summation is performed using a custom-made post-processing script by rotating each dose map (Figure 3c) and resampling them into 0.005 × 0.005 × 1 mm^3 dose bins (Figure 3d) and summing each incidence to create a unique high-resolution dose map. Furthermore, another set of scripts dedicated to dose metrics and planning analysis, which allows us to extract peak and valley dose maps separately based on the extraction method described by Ocadiz et al.[17] Extracted peak and valley dose maps, could be used for dose prescription and absolute dose calculation and also comparisons with lower resolution peak and valley dose maps as obtained with the hybrid algorithm.[37]

The same set of scripts allows us to go beyond the state of the art in dose metrics adapted to MRT. Typically in MRT peak (efficacy) and valley (toxicity) dose values have been studied as well as 1D dose metrics such as dose profiles or percentage depth dose (PDD) curves. The PVDR is also used as a quality indicator that qualifies the microbeam dose distribution with one number.[52] By using penMRT and high-resolution dose maps, we were able to develop high-resolution differential dose–volume histograms (dDVHs) and cumulative DVHs (cDVHs) in order to propose dose metrics that

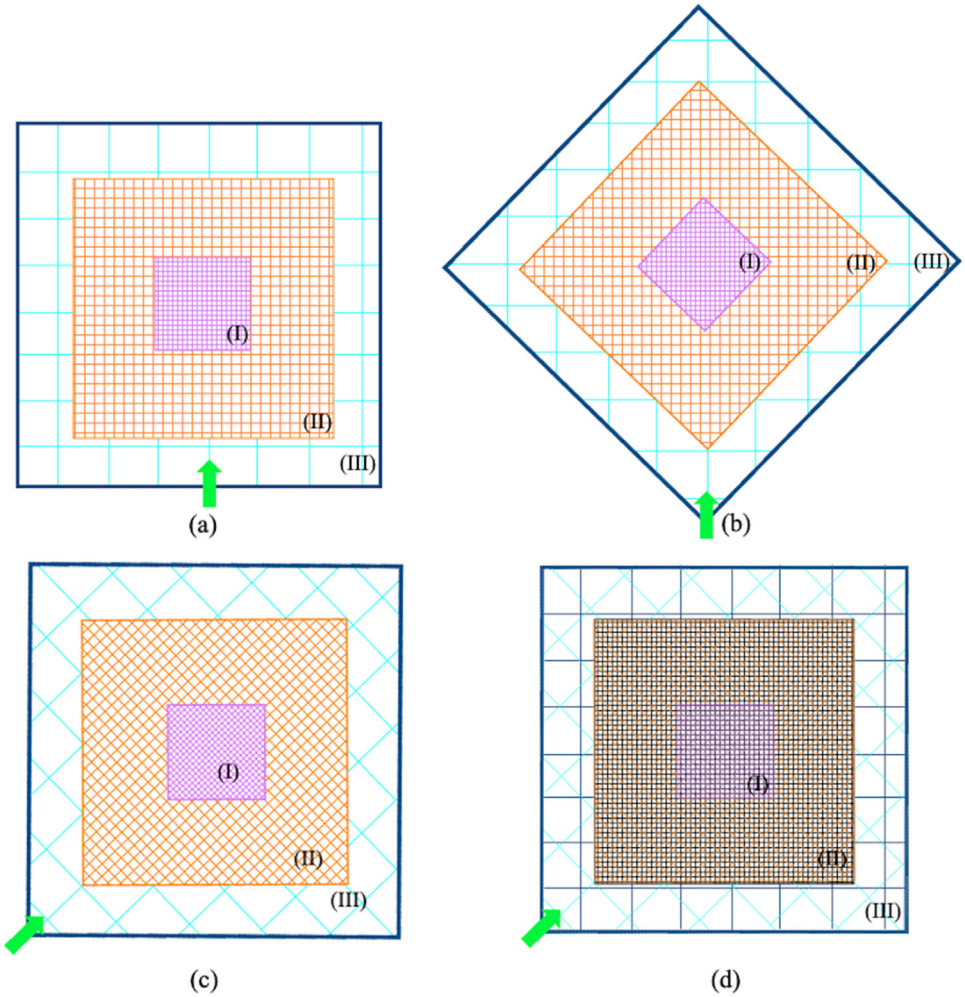

FIGURE 3 Multi-scale dose calculation grid configuration. The green arrow represents the direction of the incident beam. Zone (I), zone (II), and zone (III) represent the high-, medium- and low-resolution regions, respectively. (a) An example of multi-scale dose calculation grid in which the dose information in the beam entrance and after the target is not needed to be rendered at a micrometric resolution. The high-resolution calculation grid is confined to the center of the phantom. (b) Same as "a" but with a 45 degrees beam angle. The grid is rotated to remain perpendicular to the beam axis. (c) The dose map obtained in the "b" configuration is rotated to be presented in the same coordinates as the reference orientation. (d) Post-processing operation performed on the dose map shown in "c"; the dose map is resampled to be presented in an orthonormal grid

provide a clear rendering of the dose distribution complexity in MRT and tools for advanced treatment plan evaluation.

2.4 | Cross-validations and performance tests on penMRT

Benchmarking of penMRT against penmain and Gate. As penMRT has been developed by modifying significantly a structured general-purpose main program from PENELOPE, it must be first validated against the already benchmarked reference code penmain. In order to compare to an independent MC code, it has been decided to use Gate (version 8.2).[53] Thus, a series of cross-validation tests have been performed, based on dose maps, PDDs and dose profiles analysis, in order to validate penMRT. For comparison purposes, apart from the intrinsic differences in source geometry definition between Gate and PENELOPE and the chosen physics list, the same simulation parameters have been used in Gate rather than in penmain and penMRT. Indeed, in order to take into account the polarization effect, in Gate the "Livermore_polar" physics list has been used.

The spectrum which has been used by Martínez-Rovira et al. in 2011[20] has been used for these cross-validations (average energy of 103.8 keV, see Figure 2). As the goal of this work is to validate the reliability of penMRT, no variance reduction methods were used. Even if the beam divergence is negligible for synchrotrons X-rays; the small beam divergence has been taken into account in this study by positioning the radiation source 40.5 m away from the center of the phantom.[20]

Performance tests on penMRT consist in comparing Gate, penmain and penMRT for various combinations of C1 and C2 values:

1. For irradiations with a rectangular homogeneous 2×2 cm^2 radiation field (broad beam): Penmain and Gate simulations were done in a quadric (Figure 2a) water phantom ($18 \times 18 \times 18$ cm^3) and were manually parallelized on 10 CPUs. PenMRT simulations were carried out on a voxelized (Figure 2b) water phantom ($18 \times 18 \times 18$ cm^3) with the parallelization performed using OpenMPI on 10 CPUs. To have an acceptable uncertainty, 1010 particles are simulated. Doses were scored in bins of $0.5 \times 1 \times 1$ mm^3 and a zone of 180 (X direction) $\times$ 180 (Y direction) $\times$ 180 (Z direction) mm^3 centered at the center of the radiation field was covered by the dose grid. The calculation was done in about 1.2×10^7 voxels.
2. For irradiations using a single microbeam (50 μm $\times$ 2-cm radiation field) in quadric and voxelized water phantom (Figure 2): The simulation parameters and parallelization are the same as in "1.". The comparisons were done on a single microbeam, because both penmain and Gate are neither capable of replicating the radiation source nor take into account the huge number of voxels which is necessary to cover the entire radiation field. Doses were scored in bins of $0.005 \times 1 \times 1$ mm^3, where the 0.005-mm dimension is perpendicular to the microbeam axis. A zone of 0.8 (X direction) $\times$ 180 (Y direction) $\times$ 30 (Z direction) mm^3 centered at the center of the irradiation field was covered by the dose calculation grid. The calculation was done in about 1.3×10^6 voxels.

The results obtained by penmain, Gate and penMRT are compared by using the relative difference given by

$$\delta = \frac{D_{penMRT} - D_{ref(penmain/Gate)}}{D_{ref(penmain/Gate)}} \quad (1)$$

where D is the calculated dose in each dose bin, with the reference values being set to the penmain and Gate results.

The 2D dose maps evaluation was carried out by the gamma index test, which is a pass–fail test using an ellipsoid of acceptance. The test is defined as follows[54]:

$$\Gamma(r, D) = \sqrt{\frac{\Delta r^2}{\Delta d_M^2} + \frac{\Delta D^2}{\Delta D_M^2}} \leq 1 \quad (2)$$

where ΔD_M and Δd_M are the acceptance criteria for the dose difference and the distance to agreement (DTA), respectively. If $\Gamma(r, D)$ stands between 0 and 1, the test passes, otherwise it fails. In our study, the dose map calculated by penmain (C1 = C2 = 0.1) is taken as a reference.

Performance tests of penMRT. Four distinct performances tests have been performed to study the capacities of penMRT for:

1. Dose profiles and depth doses curves for the study of monodirectional irradiations:

The abovementioned X-ray spectrum has been used (average energy of 103.8 keV). The simulations were performed using a conservative C1 and C2 value of 0.05. The source is an array of 51 microbeams (50 μm wide, 2 cm height), covering a 2×2 cm^2 field (400 μm spacing, center to center). A zone of 3 (X-direction) $\times$ 18 (Y-direction) $\times$ 3 (Z-direction) cm^3 is covered with a high-resolution dose grid, where X is the horizontal direction perpendicular to the incident beam, Z is the vertical direction and Y is the beam propagation direction. This ensures a high-resolution coverage of the whole beam path. The doses were scored in bins of 0.005 (X-direction) $\times$ 1 (Y-direction) $\times$ 1 (Z-direction) mm^3. 2×10^9 primary particles have been simulated on 80 CPUs. In this case, the calculation was done in 3.367×10^7 micrometric bins, more than 7.5×10^5 millimetric bins, and around 1300 centimetric bins, to cover all areas of interest in the simulation universe (water phantom and air around the phantom). The dose maps given by penMRT have also been benchmarked with penmain and Gate. As the simulation of an array of microbeams in the same condition as penMRT was not possible, a single microbeam was simulated in penmain and Gate. The absorbed doses were scored on a zone of 5 (X-direction) $\times$ 6 (Y-direction) $\times$ 3 (Z-direction) cm^3 in the pixels of 0.005 (X-direction) $\times$ 1 (Y-direction) $\times$ 1 (Z-direction) mm^3. The obtained dose map was replicated 51 times with a pitch of 400 μm and summed to simulate the 2×2 cm^2 field.

2. Source replication approach validation

In order to validate the source replication strategy against a full modeling of the mulitslit collimator, a simulation of the irradiation geometry has been performed with the MSC based on Martínez-Rovira et al.[20] calculations and compared to the source replication method in penMRT. The point source has been set at 40.5 m from the sample. The MSC is defined according to Bräuer-Krisch et al.[50] and placed 1 m behind the sample. The simulations were performed using a harder spectrum, which is currently used for preclinical tests at the ESRF-ID17,[20,55] on large animals (121.7 keV average energy) to be in the worst transmission situation. The following parameters are used C1=C2 = 0.05, absorption energies of 10 keV and 1 keV for photons and electrons, respectively. The dose calculation grid resolution is set to $0.005 \times 1 \times 1$ mm^3. A 410 μm center-to-center pitch for the source replication has been used for this comparison to account for the beam divergence

in the simulation with a point source and collimator in place.

3. Cross-fired irradiation validation:

For benchmarking penMRT against penmain in cross-fired irradiation geometries. A single microbeam of 50 μm × 2 cm in a water phantom of 18 × 18 × 18 cm^3 is simulated with the same spectrum as "2." and the doses are scored using the grids of 0.005 × 1 × 1 mm^3 on a zone of 5 × 6 × 3 cm^3. This dose map is then replicated with a pitch of 400 μm to simulate the 2 × 2 cm^2 field. For each incidence angle, the dose maps are resampled (using grid data from the SciPy package) to obtain 0.005 × 0.005 × 1 mm^3 dose bins and summed for each incidence. The same process of resampling and summation has been performed on penMRT dose maps. A 1 × 1 × 0.1 cm^3 region of interest (ROI) is chosen at the center of the dose maps for statistical comparison purposes. The similarity of dose distributions is investigated using a statistical Q–Q test (quantile–quantile plot) on the dDVHs that are calculated on the ROI. The comparisons have been performed for the cross-fired irradiation protocol with two beams at 90 degrees.

4. Cross-fired irradiations using several microbeam arrays:

The simulations were performed using the same spectrum as "2." and C1 and C2 were kept to a conservative value of 0.05. A dose calculation grid configuration is chosen in order to study the cross-firing region with a high-resolution (Figure 3a). A zone of 3 (*X*-direction) × 6 (*Y*-direction) × 3 (*Z*-direction) cm^3 at the center of an 18 × 18 × 18 cm^3 water phantom was covered with the high-resolution dose calculation grid of 0.005 (*X*-direction) × 1 (*Y*-direction) × 1 (*Z*-direction) mm^3, where *X* is the horizontal axis perpendicular to the incident beam. The remaining geometry was covered by a 1 × 1 × 1 mm^3 dose calculation grid. The phantom was irradiated with a single (at 0°) and three (at 0°, 35°, and 90°) irradiation beams. This performance test highlights the multi-scale capabilities of penMRT as well as its capacity to simulate multi-directional treatments. The different beam incidences were simulated separately using 2 × 10^9 particles on 80 CPUs within more than 1.1 × 10^7 micrometric bins, 6 × 10^6 millimetric bins and 1300 centimetric bins.

The summed dose maps are thus obtained and displayed in 0.005 × 0.005 × 1 mm^3 voxels in the abovementioned high-resolution region, after rotation of each individual dose map. High-resolution dDVHs are extracted on a 1 × 1 × 1 cm^3 ROI centered on the treatment isocenter at the center of the phantom.

3 | RESULTS

3.1 | PenMRT versus penmain and Gate cross-validation tests

Broad beam irradiation fields. For both, penMRT and penmain, simulation times of around 120, 50, and 36 h were recorded on the ESRF cluster[56] to simulate 10^{10} primary showers, for C1 and C2 values of 0.01, 0.05, and 0.1, respectively (by doubling the C1 and C2 parameters, the simulation time decreases by a factor of 3.5). In the case of Gate, the simulation time was about 72 h.

Isodose maps, gamma index maps and dose profiles calculated by penmain, Gate and penMRT in a phantom irradiated by a broad beam of 2 × 2 cm^2 are compared at a depth of 2 cm in water in Figure 4. The doses obtained with penmain using C1 and C2 values of 0.01 are taken as a conservative reference value compared to C1, C2 equal to 0.05 and 0.1 as suggested by Salvat et al.[39] and Martínez-Rovira et al.,[22] respectively.

The 2D evaluation (2%, 1 mm relative gamma index test, Figure 4a) shows a gamma index passing rate of 99% within the isodose of 20%. The vertical deformation of the 5% isodose in Figure 4a highlights that the polarization effect has been properly taken into account. In Figure 4b and d, the comparison of horizontal and vertical dose profiles between penmain, Gate and penMRT are showing an excellent agreement regardless of the C1 and C2 values. The comparison between the vertical and horizontal dose profiles shows the polarization effects on field edges and out-of-field doses. A maximum polarization of synchrotron generated X-rays in the horizontal direction, causes a diminution of the out-of-field dose in the horizontal plane and an increase in the vertical plane. The polarization effect leads to similar results for penmain, Gate and penMRT (Figure 4d). The relative differences are plotted only for C1 and C2 equal to 0.01, 0.1, and Gate, for not overcharging Figure 4c and e. Figures s 4c and e show that the relative difference is less than ±0.5% inside the irradiation field. The relative differences outside the irradiation field, beyond the 10% isodose, are higher and can reach a maximum of about ±10%, due to the significant increase of the intrinsic statistical uncertainties. A two sigma uncertainty level of 0.9%, 0.9% and 2.3% have been achieved in the beam center, penumbra and out-of-field (1.5 cm from the beam center), respectively.

The experimental doses as measured with a pinpoint ionization chamber agree with the doses calculated with penMRT and relative differences between 0.15% and 1.5% are measured for depths ranging from 2 to 10 cm in solid water.

Single microbeam irradiation fields. For cross-validation of penMRT versus penmain and Gate in micrometric scale, simulation times of around 38, 19, and 8 h were recorded on the ESRF cluster, to simulate

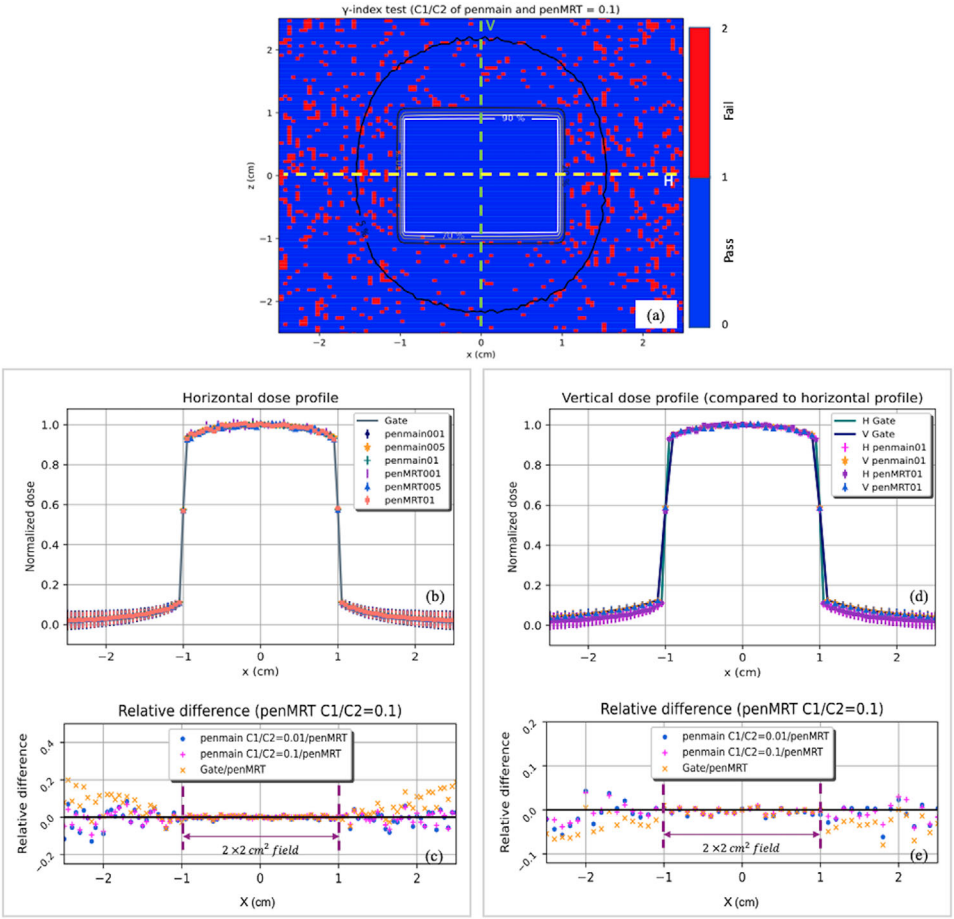

FIGURE 4 Cross-validation of dose maps and dose profiles obtained by penmain, Gate and penMRT in a water phantom irradiated by a 2 × 2 cm^2 broad beam field at a depth of 2 cm. (a) 2%/1 mm relative gamma index test where the dose map of penmain as the reference is compared to penMRT (C1 = C2 = 0.1). (b) Comparison of horizontal dose profiles, (c) Relative difference between horizontal dose profiles obtained by penMRT, penmain, and Gate (reference: penmain with C1 = C2 = 0.01, 0.1 and Gate, respectively.) (d) Comparison of vertical and horizontal dose profiles obtained with penMRT, penmain (C1 = C2 = 0.1) and Gate. (e) Relative difference between vertical dose profiles obtained by penMRT, penmain and Gate (reference: penmain with C1 = C2 = 0.01, 0.1 and Gate, respectively)

10^{10} primary showers, for C1 and C2 values of 0.01, 0.05, and 0.1, respectively. In the case of Gate the simulation time was about 48 h.

Isodose maps, gamma index maps and dose profiles calculated by penmain, Gate and penMRT in a phantom irradiated by a single microbeam of 50 μm × 2 cm are compared at a depth of 2 cm in water in Figure 5. The values obtained with penmain using C1 and C2 values of 0.01 are chosen as a conservative reference. A 100% passing rate for a relative gamma index test of 2%/5 μm is obtained (Figure 5a). The relative difference in the doses calculated by penmain, and penMRT stays lower than 0.1% in the microbeam, and stays below 1% until the 5% isodose (Figure 5c) due to the statistical uncertainty increase. A two sigma uncertainty level of 0.2%, 0.3% and 4.8% has been achieved in the microbeam center, penumbra (the distance between 80% and 20% of the peak dose) and out-of-field (175 μm from the microbeam center), respectively.

Gate and penMRT comparison. Comparisons between Gate and penMRT show good agreement inside the irradiation field (differences lower than 0.1%). This accordance decreases at the field edges which can be explained by the different strategies in source definition in these two separate simulations and by the use of different physical models. The differences in the physics lists can introduce discrepancies between the two simulations (around 10%–15% for the broad beam, and around 5% for the single microbeam). These out-of-field or valley doses are mainly due to scattered photons and electrons transport. This difference in out-of-field doses calculated by PENELOPE and Livermore is also reported in other studies.[57]

PDDs in broad beam and single microbeam fields. The PDD simulated for broad beams and one microbeam, using penmain, Gate and penMRT at various values of C1 and C2 are represented in Figure 6. A good agreement between penmain and

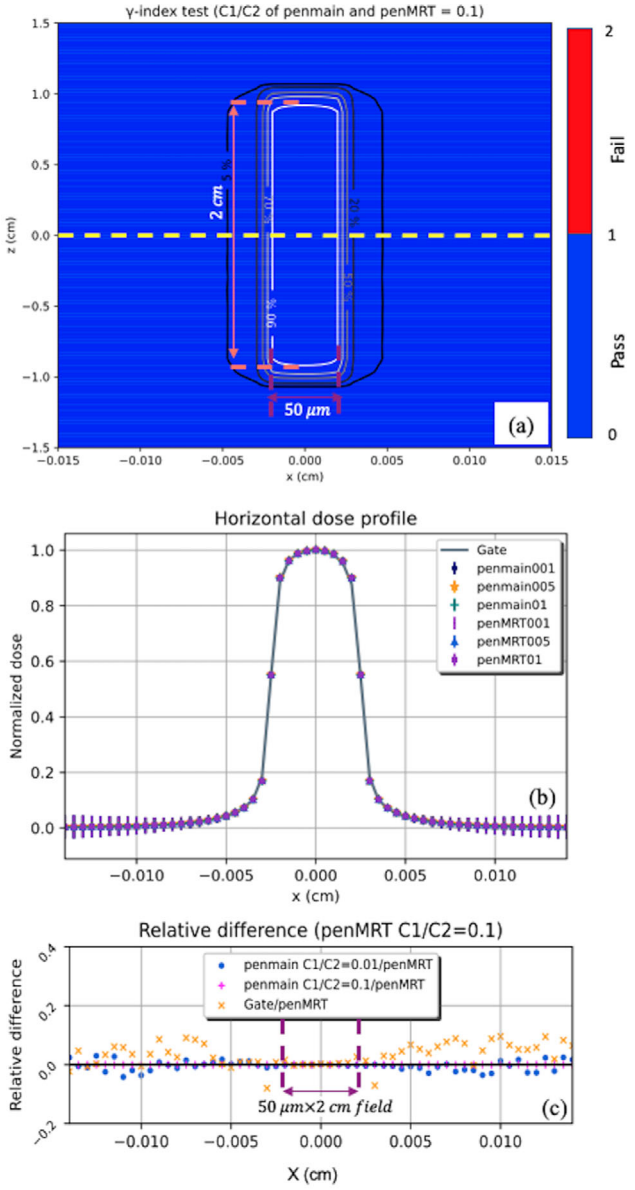

FIGURE 5 Cross-validation of dose maps obtained by penmain, Gate, and penMRT in a water phantom irradiated by a 50 μm × 2 cm single microbeam field. (a) Relative gamma index test of 2%/5 μm where the dose map of penmain as the reference is compared to penMRT (C1 = C2 = 0.1). (b) Horizontal profiles were obtained by penMRT, Gate, and penmain. (c) Relative difference between penMRT, penmain and Gate (reference: penmain with C1 = C2 = 0.01, 0.1 and Gate, respectively)

penMRT is observed for broad beam PDDs (Figure 6a and b), with a maximum relative difference of ±1.5% in depth below 12.5 cm (which corresponds to the isodose 20%) and showing an increase in the statistical uncertainty coherent with the depth increase. An excellent agreement is observed between penmain and penMRT for a single microbeam. A maximum relative difference of less than ±1% is observed, independently of the considered depth (Figure 6c and d), because in that case, the 10^{10} particles are concentrated in the microbeam. As is shown in Figure 6b and d a relative difference lower than 1% is observed between penmain, Gate, and penMRT. The discrepancies increase with depth to reach 6% and it might be due to the differences in the physical models in these two approaches.

3.2 | PenMRT performance characterization

Full MRT field simulation. After benchmarking penMRT against penmain for broad beam and single microbeam simulations, the performance of penMRT was tested in full irradiation field of 2 × 2 cm^2 consisting of an array of 51 microbeams (50 μm by 20 mm equally spaced, 400 μm center to center). In this case, a simulation time of 28 h was recorded on the ESRF cluster (2 × 10^9 primary particles, dose calculation grid of 0.005 × 1 × 1 mm^3). A two sigma uncertainty level of 1.1%, 3%, and 6% has been achieved in the beam center, penumbra, and valley area (average of 100 μm centered at the valley center), respectively.

The dose map at 2 cm of depth, the horizontal dose profile in the center of the field, as well as the peak and valley PDDs are represented in Figure 7. The PDD values (Figure 7c and d) correspond to doses averaged on 0.01 × 1 × 1 mm^3 bins for the peak PDD, 0.1 × 1 × 1 mm^3 for the valley PDD. The peak dose PDD is varying as a decreasing mono-exponential function with depth. PDD(y) = 100exp (−0.16084y), so the calculated linear attenuation coefficient is 0.1608 cm^{-1}, while the linear attenuation coefficient of water at 103.8 keV is 0.1687 cm^{-1}, which is less than 5% difference, using the monochromatic approximation. The valley doses are mainly caused by the scattered photons from the peaks inside the field. We observe that the valley doses increase to a maximum value and then decrease with the depth. This depth depends on the energy spectrum and in our case the maximum valley dose appeared at a depth of 1.9 cm. The valley PDD also exhibits a higher statistical uncertainty as valley doses are only made of out-of-field doses.

The dose map obtained with penMRT is compared to the dose map obtained by replicating the dose maps obtained by penmain and Gate with one single microbeam (Figure 8). There is a good agreement in the peaks doses (less than 1% relative difference), whilst the valley doses differ from 0.5% to 7.5 % between Gate and penMRT, which could be due to the differences in the physics lists that impact the modeling of the transport of low-to-medium energy photons and electrons.

In order to justify the usage of the source replication model, an MRT dose profile obtained by replication is compared to an MRT dose profile obtained by simulating the MSCs (a zoom on the central peak and valley is shown in Figure 9).

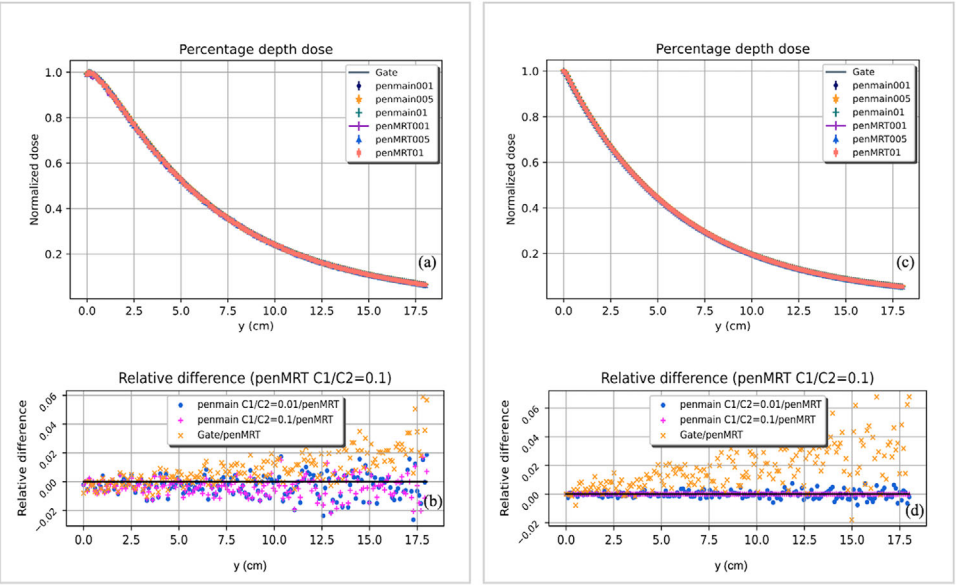

FIGURE 6 (a) PDDs in broad beam obtained by penmain and penMRT with C1 and C2 values of 0.01, 0.05, and 0.1 and Gate. (b) Relative difference between PDD of penMRT/penmain (reference: penmain with C1 = C2 = 0.01 and 0.1) and penMRT/Gate in the broad beam. (c) PDDs in a single microbeam obtained by penmain and penMRT, with C1 and C2 values of 0.01, 0.05, and 0.1 and Gate. (d) Relative difference between the PDD obtained by penMRT/penmain (reference: penmain with C1 = C2 = 0.01 and 0.1) and penMRT/Gate in the single microbeam. PDD, percentage depth dose

By using the source replication approach, we have about 0.6% dose underestimation on valleys, due to the lack of scattering and transmission effects on MSCs blades. At the peak center, the relative difference is negligible. A 5%–10% relative difference is observed in high-gradient areas, that is in the microbeam penumbras over 15 μm. This is inherent to the source definition strategy. This validates the source replication approach, neglecting the collimator transmission and scatter effects.

3.3 | Multi-scale dose maps in unidirectional and multidirectional MRT irradiations

Before testing penMRT in complex treatment conditions, penMRT has been validated against penmain for multidirectional irradiations.

The comparisons between penmain and penMRT for multiple incidences of irradiations are represented in Figure 10. As the Q–Q test has returned a dose comparisons distributions map that follows the $y = x$ line, it clearly shows the similarity of the two-dose distributions. We thus validated penMRT against penmain for microbeam arrays for multiple incidences.

In the end, all implemented features in penMRT were tested by simulating unidirectional, bidirectional and multidirectional treatments. Figure 11 shows the multi-scale dose maps along with a zoom on the high-resolution calculation grid. Simulating each beam requires less than 24 h on the ESRF cluster. In multidirectional treatment, all the treatment beams can be simulated at the same time. Showing micrometric information on a centimetric scale induces some display artifacts which are visible in the subplots of Figure 11. The dose values are however available as shown on the zoomed figure, where display artifacts are no longer seen.

The interpretation of high-resolution dose maps can be helped by the analysis of high-resolution DVHs. An example of high-resolution DVHs obtained on a virtual $1 \times 1 \times 1$ cm^3 target centered on the treatment isocenter is also shown in Figure 11. The dose was prescribed such that the whole ROI received a minimum valley dose of 1 Gy in each irradiation beam. The minimum value of DVHs is 1 and 3 Gy, for unidirectional and 3 beams treatments, respectively. The bin width on the DVHs is set at 1 Gy. The peak doses are leading to bell shape plots on the DVHs with the presence of stripes of peak doses as well as hot spots where microbeams cross. To our knowledge, these are the first high-resolution dose maps and DVHs obtained for MRT treatments using cross-fired beams.

In unidirectional treatments (Figure 11a.III), 70% of the target receives valley doses from 1 to 4 Gy, whilst around 9.8% of the volume receives the peak doses (>40 Gy) and 2.32% of the volume receives the doses from the average penumbra values (20–40 Gy). Cumulative dose analysis confirms that 100% of the target benefits from the minimum valley dose (1 Gy), and around 12.5% of the volume is exposed to peak doses. In the case of two perpendicular MRT field treatments (results are not shown as they are implicitly represented in 3 beams treatment analysis), about 61.1% of the target

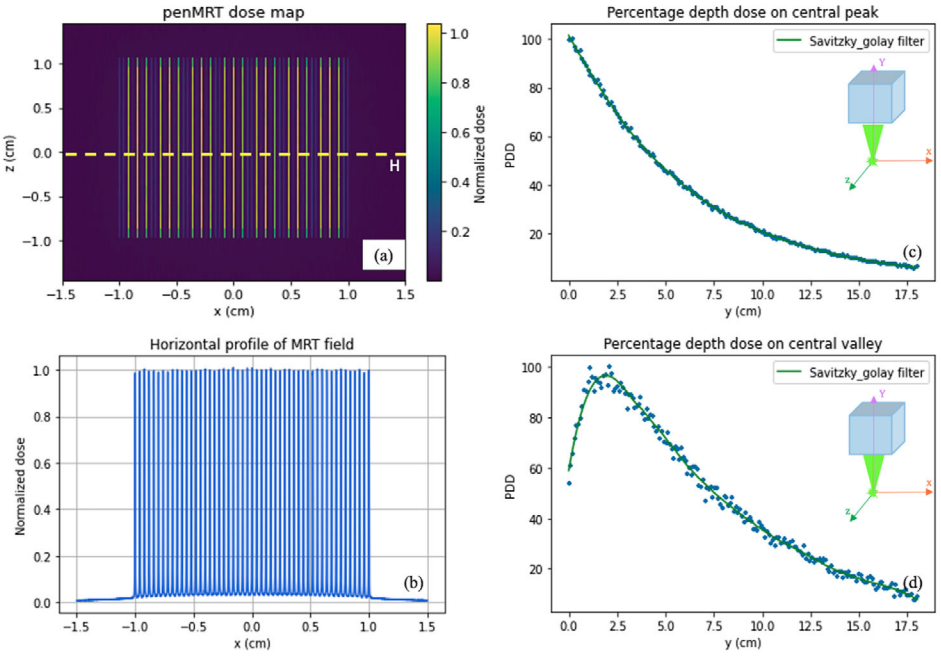

FIGURE 7 (a) Dose map for a 2 × 2 cm^2 MRT irradiation field. The position of the horizontal dose profile is shown with a dashed line. (b) Horizontal dose profile at 2 cm of depth. (c) Central peak. (d) Central valley PDD. MRT, microbeam radiation therapy; PDD, percentage depth dose

receives the sum of the two valley doses (2–8 Gy), whilst about 1.28% of the volume receives the sum of 2 peak doses (>90 Gy). Overall, 16.51% of the volume receives the doses which come from one peak and one valley (around 55 Gy). Cumulative dose analysis shows that 20%–23% of the volume is exposed to lethal doses if the latter are equal to at least one peak dose. In the MRT treatment based on three fields (Figure 11b.III), the percentage of the volume receiving the doses from three valleys decreases to about 46%. About 0.1% of the volume has the dose of three covering peaks, whilst 0.31% of the volume takes advantage of two covering peaks and about 17% of the volume receives the dose of two valleys and one peak. Based on cumulative dose analysis 100% of the volume receives at least the three valley doses and at 30%–35% of the target, volume is covered by lethal doses brought by at least one peak.

4 | DISCUSSION

In this paper, penMRT has been first benchmarked against penmain and Gate for broad beam calculations as well as for a single microbeam irradiation and a full microbeam array. This benchmarking was mandatory to test the fact that the modifications performed in the PENELOPE general-purpose main program penmain[39] to build penMRT were not affecting the accuracy of the MC simulations themselves. This has been validated for various values of C1–C2 from 0.01 to 0.1, respectively. The source replication approach and multidirectional treatment have also been validated.

The penMRT performance tests demonstrate the reliability of penMRT to be used for 3D conformal MRT irradiations. In Table 2, the PVDRs obtained by penMRT are compared to the PVDR available in the literature. The penMRT calculated PVDR values in a square field composed of an array of 51 microbeams, and are in good agreement (0%–8% relative difference) with the study conducted by Martínez-Rovira et al. in 2012 with an approach limited to one unidirectional square field irradiation at a normal incidence to the voxelized phantom.[22] The study from Martínez-Rovira et al.[22] is based on a complete simulation of the beamline components (from wiggler to phantom), while penMRT is based on an approach that aims at optimizing the simulation time without impairing the results such as the source replication and the use of MRT spectra as generated by the Oasys software[58] developed at the ESRF. It was thus essential to compare the two approaches in similar cases. The PVDR values calculated by penMRT are also compared to the hybrid dose calculation PVDR values given by Donzelli et al.[37] In this publication a spectrum with an average energy of 105 or 110 keV has been used. In our study, the small animal's spectrum with an average energy of around 103.8 keV has been used. A relative difference between 0% and 8.5% can be observed between penMRT and hybrid PVDR values. The highest differences (8.5% and 5.7%, for 5 and 10 mm depth, respectively) are observed mostly in the lower depths, which can be explained by differences

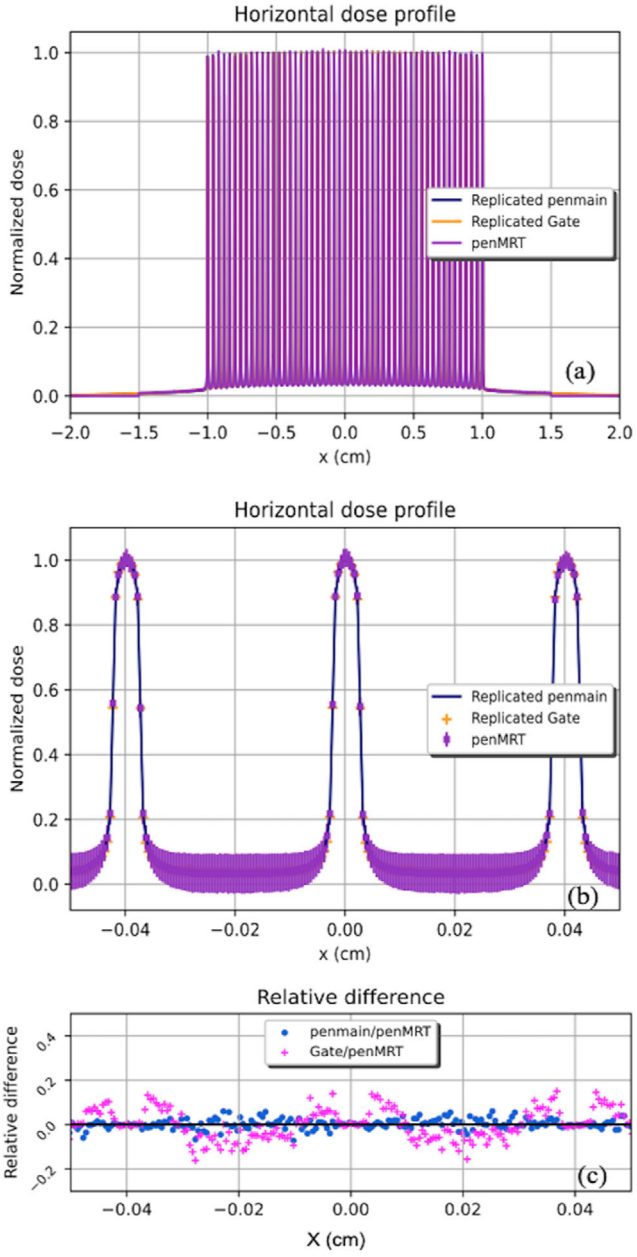

FIGURE 8 (a) Comparison of horizontal MRT profiles in a field created by penMRT and the fields created using single microbeam replication in penmain and Gate. (b) A zoom on horizontal profile. (c) The relative difference between penMRT/penmain and penMRT/Gate horizontal profiles. MRT, microbeam radiation therapy

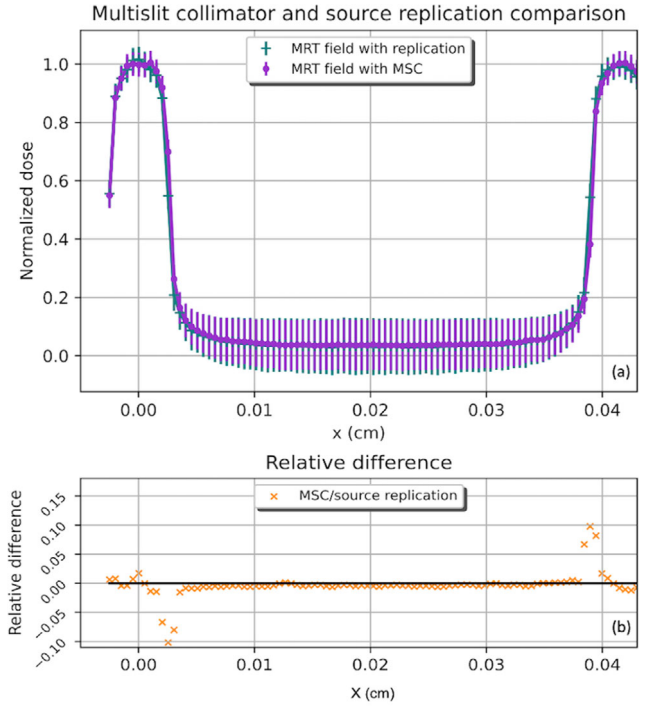

FIGURE 9 (a) Comparison of dose profiles (zoom on the central peak and valley) obtained by source replication approach and modeling a multislit collimator in a water phantom irradiated by a 2 × 2 cm^2 MRT field at a depth of 2 cm (standard deviation of two sigma is demonstrated in this figure). (b) Relative difference of dose profiles of simulated by source replication approach and multislit collimators. MRT, microbeam radiation therapy

in the low-energy spectrum components between these two studies. The results are also coherent with the experimental study performed by Livingstone et al.[10]

It is also shown that taking into account the photon polarization is important for penumbras and out-of-field doses calculations. The polarization effects should not be neglected, in particular when the prescription is performed on valley doses. Our results were in accordance with the study conducted by De Felici et al. on the polarization effect.[29]

The source replication approach used in penMRT accelerates the simulations with the cost of neglecting the transmission, diffusion, and reflection through the MSC. In a recent study from Pellicioli et al.[59] the effect of the MSC on peak and valley doses has been investigated. Based on this study, a perfect collimator assumption might cause an underestimation of the valley doses from 5% to 30% depending on the field size and the energy spectrum. The peak doses might be less affected with an underestimation of about 0.2%. The experimental valley doses values found experimentally by Pellicioli et al. might, however, be slightly overestimated due to the irradiation modality used to retrieve valley doses from HD-V2 Gafchromic films, which might have introduced a blurring effect and increased valley doses. Our source replication validation showed that the valley dose underestimation would be around 0.6%. However, in order to have an improved precision of the collimator contribution, a mother simulation can be run and a PSF after the MSC is retrieved, but loading and processing a PSF would increase the simulation time considerably,[60] when compared to the source replication approach. As an alternative, simulating the contribution of multislit blades in the form of multiple virtual sources is also under investigation.

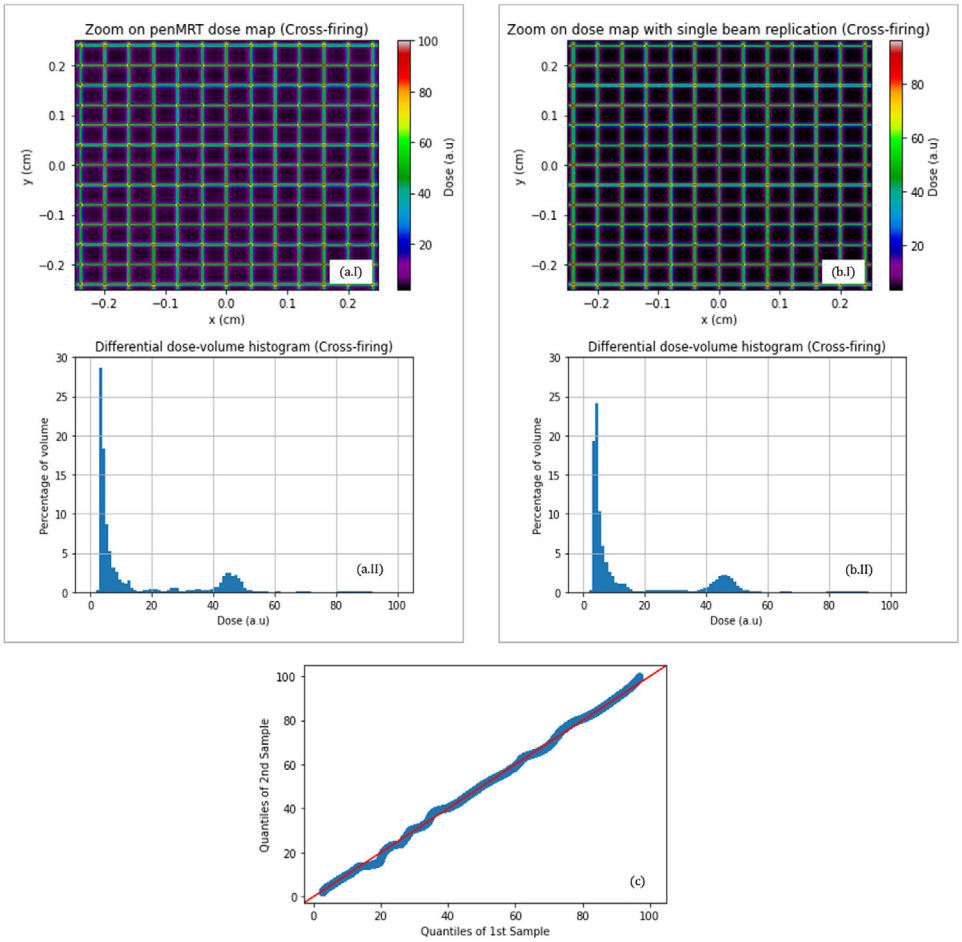

FIGURE 10 Simulation of a multi-directional treatment. (a.I) A cross-fired dose map given by penMRT. (a.II) The penMRT differential dose–volume histogram on a region of interest of $1 \times 1 \times 0.1$ cm^3. (b.I) A cross-fired dose map given by a penmain. (b.II) The penmain differential dose–volume histogram on the same region of interest. (c) Q–Q plot to investigate the similarity between (a.II) and (b.II)

In this study, the capability of penMRT to simulate high-resolution and multi-scale and multidirectional dose maps has been validated. To our knowledge, these are the first high-resolution dose maps obtained on a cross-fired irradiation scheme using synchrotron-generated microbeam arrays. The dose maps are used to extract high-resolution DVHs. This is of particular interest for treatment planning in MRT, with dose metrics representing the complexity of the irradiation. So far, the treatment plans in MRT[8,61] trials are performed using the hybrid algorithm,[37] which has a limited spatial resolution due to macroscopic rendering of separated peak and valley dose maps.[17] PenMRT enables planning and optimization of MRT treatments using high-resolution dose metrics when several microbeams arrays are used. Based on a recent hypothesis in MRT, the radiotherapy toxicity and the treatment efficiency is linked to valley and peak doses, respectively.[8,61] However, the role of the array of microbeams, the hot spots and their spatial distribution in multidirectional irradiation is still unknown. A recent study by Cahoon et al.[62] is pointing to the potential role of the bystander effects linked to the over irradiated cells in the beam passage. PenMRT's generated high-resolution dose maps and DVHs, showing the distribution at a micrometric scale of areas covered by peaks, valleys and hot spots is undoubtedly a significant added value to the study of the biological outcome of spatially fractionated radiation therapy. The next step of this work is to perform the experimental validation of penMRT using high-resolution detectors irradiated in clinical conditions through end-to-end studies with conformal fields. The use of variance reduction methods (e.g. interaction forcing) on the speed and accuracy of simulations will be also investigated.

5 | CONCLUSION

We have developed a multi-scale full MC dose calculation engine, penMRT, which allows the user to obtain dose maps at the micrometric scale for photons irradiations. This engine is optimized for microbeam radiotherapy, but it can be used in other treatment modalities, where a micrometric resolution and a large number

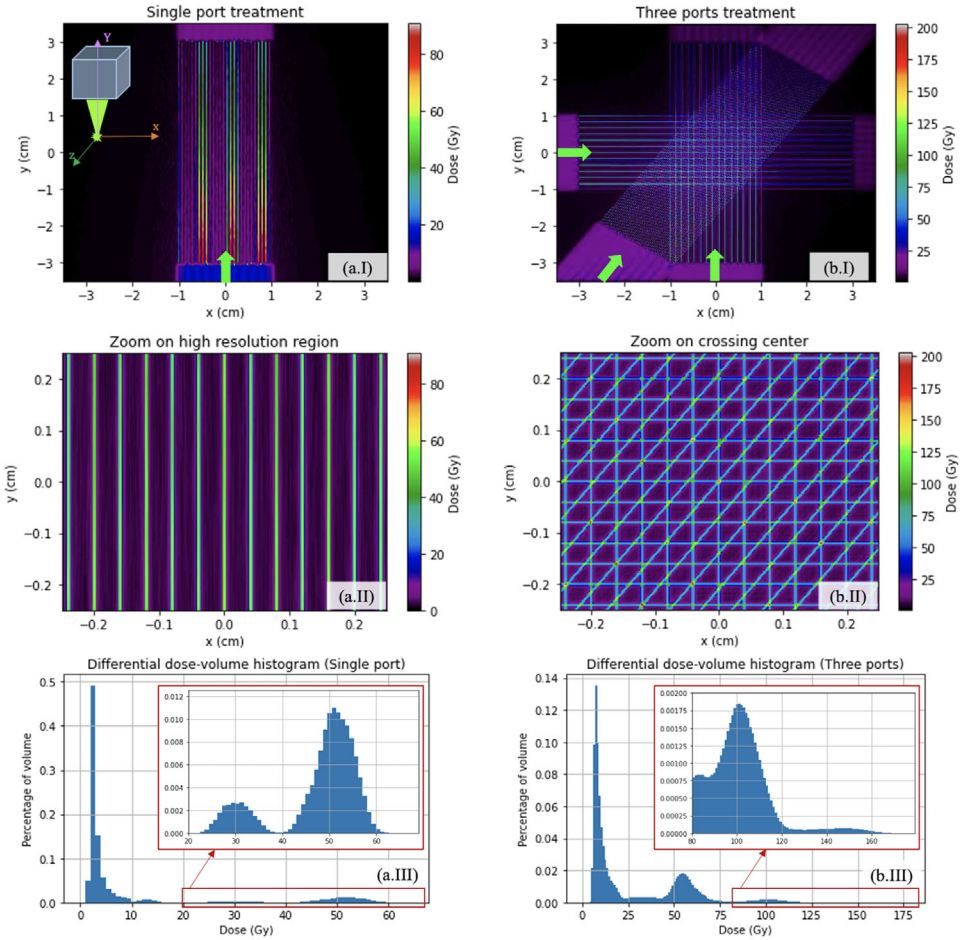

FIGURE 11 Dose maps in *X*–*Y* plan for irradiation fields of 2×2 cm^2, where *X* is the horizontal direction perpendicular to the microbeam array direction and *Y* is representing the depth dose plan. The high-resolution grid of 0.005 (*X* direction) × 1 (*Y*-direction) × 1 (*Z*-direction) mm^3 covers a $3 \times 6 \times 3$ cm^3 zone and the medium resolution dose grid of $1 \times 1 \times 1$ mm^3 covers an $18 \times 18 \times 18$ cm^3 of the water phantom. The direction of beam propagation is shown with a green arrow. (a.I) The macroscopic vision of the irradiated zone with a single MRT field showing micrometric and millimetric dose calculation grids on the same axis. (a.II) A zoom on a high-resolution region at the center of the figure. (a.III) dDVH of a ROI irradiated by a single MRT field. To have a better visualization, a zoom on higher dose region is given. (b.I) The macroscopic visualization of the irradiated zone by three MRT fields (0, 35, and 90° incidences). (b.II) A zoom on an ROI with high resolution. The dose hot spots from two and three crossing peaks can be seen here. (b.III) dDVH of an ROI in three irradiation field treatments with a zoom on higher dose area. dDVH, Differential dose-volume histogram; MRT, microbeam radiation therapy; ROI, region of interest

TABLE 2 Calculated PVDR in a 2×2 cm^2 MRT field as a function of depth compared to measured and calculated values in quasi-similar conditions reported in the literature. In order to have comparable standard deviations, PVDRs are given with two sigma

Depth (mm)	PVDR				
	Martínez-Rovira et al.[20] [a]		Livingstone et al.[10] [b]	Donzelli et al.[37] [c]	
	Monte-Carlo	Gafchromic film	MicroDiamond	Hybrid	penMRT[d]
5	42 ± 4	38 ± 6	33 ± 2	47	43 ± 5
10	33 ± 3	33 ± 5	28 ± 4	35	33 ± 3
20	28 ± 2	28 ± 4	24 ± 4	28	28 ± 2
40	25 ± 2	22 ± 3	21 ± 2	23	23 ± 2
50	–	–	21 ± 1	23	22 ± 2
100	23 ± 3	19 ± 3	19 ± 1	21	21 ± 3

Abbreviations: MRT, microbeam radiation therapy; PVDR, peak to valley dose ratio.
[a]Average energy of spectrum = 100 keV.
[b]Average energy of spectrum = 95 keV.
[c]Average energy of spectrum ≈ 105 keV.
[d]Average energy of spectrum = 103.8 keV.

of scoring dose bins are required. This code has been benchmarked against two general-purpose MC codes: penmain (based on PENELOPE) and Gate (based on Geant4). The ability of penMRT to calculate dose maps in multi-scale grids in unidirectional and multidirectional treatments has been validated. As a main result, the first high-resolution dose maps and associated DVHs ever obtained have been produced, which is bringing a significant added value to treatment planning in spatially fractionated radiation therapy.

ACKNOWLEDGMENTS

The authors acknowledge financial support from LabEx PRIMES (ANR-11-LABX-0063/ANR-1-IDEX-0007). The authors also acknowledge the support from the ESRF computing services for the access to the cluster and resources. The authors personally thank Michael Krisch and Paolo Pellicioli for their support, the fruitful discussions and the spectral data that is implemented in penMRT.

CONFLICT OF INTEREST

The authors have no conflicts to disclose.

DATA AVAILABILITY STATEMENT

The authors confirm that the data supporting the findings of this study are available within the article.

REFERENCES

1. Chargari C, Magne N, Guy JB, et al. Optimize and refine therapeutic index in radiation therapy: overview of a century. *Cancer Treat Rev*. 2016;45:58–67. https://doi.org/10.1016/j.ctrv.2016.03.001
2. Favaudon V, Caplier L, Monceau V, et al. Ultrahigh dose-rate FLASH irradiation increases the differential response between normal and tumor tissue in mice. *Sci Transl Med*. 2014;6(245):245ra93. https://doi.org/10.1126/scitranslmed.3008973
3. Eling L, Bouchet A, Nemoz C, et al. Ultra high dose rate synchrotron microbeam radiation therapy. Preclinical evidence in view of a clinical transfer. *Radiother Oncol*. 2019;139:56–61. https://doi.org/10.1016/j.radonc.2019.06.030
4. Montay-Gruel P, Corde S, Laissue JA, Bazalova-Carter M. FLASH radiotherapy with photon beams. *Med Phys*. 2022;49(3):2055–2067. https://doi.org/10.1002/mp.15222. Published online September 14, 2021:mp.15222.
5. Bouchet A, Lemasson B, Christen T, et al. Synchrotron microbeam radiation therapy induces hypoxia in intracerebral gliosarcoma but not in the normal brain. *Radiother Oncol*. 2013;108(1):143–148. https://doi.org/10.1016/j.radonc.2013.05.013
6. Bouchet A, Serduc R, Laissue JA, Djonov V. Effects of microbeam radiation therapy on normal and tumoral blood vessels. *Physica Med*. 2015;31(6):634–641. https://doi.org/10.1016/j.ejmp.2015.04.014
7. Smyth LML, Day LR, Woodford K, Rogers PAW, Crosbie JC, Senthi S. Identifying optimal clinical scenarios for synchrotron microbeam radiation therapy: a treatment planning study. *Physica Med*. 2019;60:111–119. https://doi.org/10.1016/j.ejmp.2019.03.019
8. Eling L, Bouchet A, Ocadiz A, et al. Unexpected benefits of multiport synchrotron microbeam radiation therapy for brain tumors. *Cancers (Basel)*. 2021;13(5):936. Published online 2021:16.
9. Shinohara K, Kondoh T, Nariyama N, Fujita H, Washio M, Aoki Y. Optimization of X-ray microplanar beam radiation therapy for deep-seated tumors by a simulation study. *J X Ray Sci Technol*. 2014;22(3):395–406. https://doi.org/10.3233/XST-140434
10. Livingstone J, Stevenson AW, Häusermann D, Adam JF. Experimental optimisation of the X-ray energy in microbeam radiation therapy. *Physica Med*. 2018;45:156–161. https://doi.org/10.1016/j.ejmp.2017.12.017
11. Duncan M, Donzelli M, Pellicioli P, et al. First experimental measurement of the effect of cardio-synchronous brain motion on the dose distribution during microbeam radiation therapy. *Med Phys*. 2020;47:213–222. Published online.
12. Bräuer-Krisch E, Adam JF, Alagoz E, et al. Medical physics aspects of the synchrotron radiation therapies: microbeam radiation therapy (MRT) and synchrotron stereotactic radiotherapy (SSRT). *Physica Med*. 2015;31(6):568–583. https://doi.org/10.1016/j.ejmp.2015.04.016
13. Yan W, Khan MK, Wu X, et al. Spatially fractionated radiation therapy: history, present and the future. *Clin Transl Radiat Oncol*. 2019;20:30–38. https://doi.org/10.1016/j.ctro.2019.10.0
14. Livingstone J, Stevenson AW, Butler DJ, Häusermann D, Adam JF. Characterization of a synthetic single crystal diamond detector for dosimetry in spatially fractionated synchrotron x-ray fields. *Med Phys*. 2016;43(7):4283. https://doi.org/10.1118/1.4953833
15. Bartzsch S, Corde S, Crosbie JC, et al. Technical advances in x-ray microbeam radiation therapy. *Phys Med Biol*. 2020;65(2):02TR01. https://doi.org/10.1088/1361-6560/ab5507
16. Donzelli M, Bräuer-Krisch E, Nemoz C, Brochard T, Oelfke U. Conformal image-guided microbeam radiation therapy at the ESRF biomedical beamline ID17. *Med Phys*. 2016;43(6):3157–3167. https://doi.org/10.1118/1.4950724
17. Ocadiz A, Livingstone J, Donzelli M, et al. Film dosimetry studies for patient specific quality assurance in microbeam radiation therapy. *Phys Med: Eur J Med Phys*. 2019;65:227–237. https://doi.org/10.1016/j.ejmp.2019.09.071
18. Slatkin DN, Spanne P, Dilmanian FA, Sandborg M. Microbeam radiation therapy: microbeam radiation therapy. *Med Phys*. 1992;19(6):1395–1400. https://doi.org/10.1118/1.596771
19. Martínez-Rovira I, Sempau J, Fernández-Varea JM, Bravin A, Prezado Y. Monte Carlo dosimetry for forthcoming clinical trials in x-ray microbeam radiation therapy. *Phys Med Biol*. 2010;55(15):4375–4388. https://doi.org/10.1088/0031-9155/55/15/012
20. Martínez-Rovira I, Sempau J, Prezado Y. Development and commissioning of a Monte Carlo photon beam model for the forthcoming clinical trials in microbeam radiation therapy: MC photon beam model for MRT clinical trials. *Med Phys*. 2011;39(1):119–131. https://doi.org/10.1118/1.3665768
21. Martínez-Rovira I, Prezado Y. Monte Carlo dose enhancement studies in microbeam radiation therapy. *Med Phys*. 2011;38(7):4430–4439. https://doi.org/10.1118/1.3603189
22. Martínez-Rovira I, Sempau J, Prezado Y. Monte Carlo-based treatment planning system calculation engine for microbeam radiation therapy: MC-based TPS calculation engine for MRT. *Med Phys*. 2012;39(5):2829–2838. https://doi.org/10.1118/1.4705351
23. Reynard D, Hugtenburg RP. A Monte Carlo intercomparison of peak-to-valley dose ratios and output factors for microbeam radiation therapy. *Radiat Phys Chem*. 2020;176:108980. https://doi.org/10.1016/j.radphyschem.2020.108980
24. Stepanek J, Blattmann H, Laissue JA, Lyubimova N, Di Michiel M, Slatkin DN. Physics study of microbeam radiation therapy with PSI-version of Monte Carlo code GEANT as a new computational tool. *Med Phys*. 2000;27(7):1664–1675. https://doi.org/10.1118/1.599034
25. Bartzsch S, Lerch M, Petasecca M, Bräuer-Krisch E, Oelfke U. Influence of polarization and a source model for dose calculation

in MRT: influence of polarization and source model in MRT. *Med Phys*. 2014;41(4):041703. https://doi.org/10.1118/1.4867858
26. Cornelius I, Guatelli S, Fournier P, et al. Benchmarking and validation of a Geant4–SHADOW Monte Carlo simulation for dose calculations in microbeam radiation therapy. *J Synchrotron Rad*. 2014;21(3):518–528. https://doi.org/10.1107/S1600577514004640
27. Dipuglia A, Cameron M, Davis JA, et al. Validation of a Monte Carlo simulation for Microbeam Radiation Therapy on the Imaging and Medical Beamline at the Australian Synchrotron. *Sci Rep*. 2019;9(1):17696. https://doi.org/10.1038/s41598-019-53991-9
28. Spiga J, Siegbahn EA, Bräuer-Krisch E, Randaccio P, Bravin A. The GEANT4 toolkit for microdosimetry calculations: application to microbeam radiation therapy (MRT): microbeam radiation therapy dosimetry with GEANT4. *Med Phys*. 2007;34(11):4322–4330. https://doi.org/10.1118/1.2794170
29. De Felici M, Felici R, del Rio MS, Ferrero C, Bacarian T, Dilmanian FA. Dose distribution from x-ray microbeam arrays applied to radiation therapy: an EGS4 Monte Carlo study: x-ray microbeam dose deposition: an EGS4 study. *Med Phys*. 2005;32(8):2455–2463. https://doi.org/10.1118/1.1951043
30. De Felici M, Felici R, Ferrero C, Bravin A, Tartari A, Gambaccini M. Monte Carlo assessment of peak-to-valley dose ratio for MRT. *Nucl Instrum Methods Phys Res A*. 2007;580(1):489–492. https://doi.org/10.1016/j.nima.2007.05.146
31. Orion I, Rosenfeld AB, Dilmanian FA, Telang F, Ren B, Namito Y. Monte Carlo simulation of dose distributions from a synchrotron-produced microplanar beam array using the EGS4 code system 4. *Phys Med Biol*. 2000;45(9):2497–2508. https://doi.org/10.1088/0031-9155/45/9/304
32. Hugtenburg RP, Adegunloye AS, Bradley DA. X-ray microbeam radiation therapy calculations, including polarisation effects, with the Monte Carlo code EGS5. *Nucl Instrum Methods Phys Res A*. 2010;619(1–3):221–224. https://doi.org/10.1016/j.nima.2010.01.018
33. Hanson AL, Slatkin DN, Laissue JA. In: Kollias N, Choi B, Zeng H, eds. Unidirectional x-ray microbeam radiosurgery of infantile neuraxial malignancies: estimations of tolerable valley doses. 2013:85655G. https://doi.org/10.1117/12.2004194
34. De Felici M, Siegbahn EA, Spiga J, et al. Monte Carlo code comparison of dose delivery prediction for microbeam radiation therapy. *J Phys: Conf Ser*. 2008;102:012005. https://doi.org/10.1088/1742-6596/102/1/012005
35. Debus C, Oelfke U, Bartzsch S. A point kernel algorithm for microbeam radiation therapy. *Phys Med Biol*. 2017;62(21):8341–8359. https://doi.org/10.1088/1361-6560/aa8d63
36. Poole CM, Day LRJ, Rogers PAW, Crosbie JC. Synchrotron microbeam radiotherapy in a commercially available treatment planning system. *Biomed Phys Eng Express*. 2017;3(2):025001. https://doi.org/10.1088/2057-1976/aa5f1a
37. Donzelli M, Bräuer-Krisch E, Oelfke U, Wilkens JJ, Bartzsch S. Hybrid dose calculation: a dose calculation algorithm for microbeam radiation therapy. *Phys Med Biol*. 2018;63(4):045013. https://doi.org/10.1088/1361-6560/aaa705
38. Day LRJ, Donzelli M, Pellicioli P, et al. A commercial treatment planning system with a hybrid dose calculation algorithm for synchrotron radiotherapy trials. *Phys Med Biol*. 2021:66:055016.
39. Salvat F, Fernandez-Varea JM, Sempau J. *PENELOPE-2018: A Code System for Monte Carlo Simulation of Electron and Photon Transport (Issy-les-Moulineaux: OECD Nuclear Energy Agency)*. 2019.
40. Rogers DWO. Fifty years of Monte Carlo simulations for medical physics. *Phys Med Biol*. 2006;51(13):R287–R301. https://doi.org/10.1088/0031-9155/51/13/R17
41. Sempau J, Badal A, Brualla L. A PENELOPE-based system for the automated Monte Carlo simulation of clinacs and voxelized geometries-application to far-from-axis fields: automated MC simulation of clinacs with PENELOPE. *Med Phys*. 2011;38(11):5887–5895. https://doi.org/10.1118/1.3643029
42. Benmakhlouf H, Bouchard H, Fransson A, Andreo P. Backscatter factors and mass energy-absorption coefficient ratios for diagnostic radiology dosimetry. *Phys Med Biol*. 2011;56:7179–7204.
43. Bartzsch S, Oelfke U. A new concept of pencil beam dose calculation for 40–200 keV photons using analytical dose kernels. *Med Phys*. 2013;40(11):111714. https://doi.org/10.1118/1.4824150
44. Wang XJ, Miguel B, Seuntjens J, Fernández-Varea JM. On the relativistic impulse approximation for the calculation of Compton scattering cross sections and photon interaction coefficients used in kV dosimetry. *Phys Med Biol*. 2020;65(12):125010. https://doi.org/10.1088/1361-6560/ab8108
45. Moskvin V, Timmerman R, DesRosiers C, et al. Monte Carlo simulation of the Leksell Gamma Knife®: II. Effects of heterogeneous versus homogeneous media for stereotactic radiosurgery. *Phys Med Biol*. 2004;49(21):4879–4895. https://doi.org/10.1088/0031-9155/49/21/003
46. Sempau J, Andreo P. Configuration of the electron transport algorithm of PENELOPE to simulate ion chambers. *Phys Med Biol*. 2006;51(14):3533–3548. https://doi.org/10.1088/0031-9155/51/14/017
47. Bernal MA, Liendo JA. An investigation on the capabilities of the PENELOPE MC code in nanodosimetry: PENELOPE code in nanodosimetry. *Med Phys*. 2009;36(2):620–625. https://doi.org/10.1118/1.3056457
48. Stewart RD, Wilson WE, McDonald JC, Strom DJ. Microdosimetric properties of ionizing electrons in water: a test of the PENELOPE code system. *Phys Med Biol*. 2002;47(1):79–88. https://doi.org/10.1088/0031-9155/47/1/306
49. Bueno G, Déniz O, Carrascosa CB, Delgado JM, Brualla L. Fast Monte Carlo simulation on a voxelized human phantom deformed to a patient: fast MC simulation on a deformed human phantom. *Med Phys*. 2009;36(11):5162–5174. https://doi.org/10.1118/1.3245877
50. Bräuer-Krisch E, Requardt H, Brochard T, et al. New technology enables high precision multislit collimators for microbeam radiation therapy. *Rev Sci Instrum*. 2009;80(7):074301. https://doi.org/10.1063/1.3170035
51. Cruise RB, Sheppard RW, Moskvin VP, *Parallelization of the Penelope Monte Carlo Particle Transport Simulation Package*. Published online 2003:11.
52. Bräuer-Krisch E, Serduc R, Siegbahn EA, et al. Effects of pulsed, spatially fractionated, microscopic synchrotron X-ray beams on normal and tumoral brain tissue. *Mutat Res/Rev Mut Res*. 2010;704(1–3):160–166. https://doi.org/10.1016/j.mrrev.2009.12.003
53. Sarrut D, Bardiès M, Boussion N, et al. A review of the use and potential of the GATE Monte Carlo simulation code for radiation therapy and dosimetry applications: GATE for dosimetry. *Med Phys*. 2014;41(6Part1):064301. https://doi.org/10.1118/1.4871617
54. Depuydt T, Van Esch A, Huyskens DP. A quantitative evaluation of IMRT dose distributions: refinement and clinical assessment of the gamma evaluation. *Radiother Oncol*. 2002;62(3):309–319. https://doi.org/10.1016/S0167-8140(01)00497-2
55. Requardt H, Bravin A, Prezado Y, et al. The clinical trials program at the ESRF biomedical beamline ID17: status and remaining steps. *AIP Conf Proc*. 2010;1234:161–164. https://doi.org/10.1063/1.3463164
56. https://www.esrf.fr/Infrastructure/Computing/NICE/Implementation
57. Cornelius I, Guatelli S, Fournier P, et al. Benchmarking and validation of a Geant4–SHADOW Monte Carlo simulation for dose calculations in microbeam radiation therapy. *J Synchrotron Rad*. 2014;21(3):518–528. https://doi.org/10.1107/S1600577514004640

58. http://ftp.esrf.eu/pub/scisoft/Oasys/readme.html
59. Pellicioli P, Donzelli M, Davis JA, et al. Study of the X-ray radiation interaction with a multislit collimator for the creation of microbeams in radiation therapy. *J Synchrotron Rad*. 2021;28(2):392–403. https://doi.org/10.1107/S1600577520016811
60. Townson RW, Jia X, Tian Z, Graves YJ, Zavgorodni S, Jiang SB. GPU-based Monte Carlo radiotherapy dose calculation using phase-space sources. *Phys Med Biol*. 2013;58(12):4341–4356. https://doi.org/10.1088/0031-9155/58/12/4341
61. Coquery N, Adam JF, Nemoz C, et al. Locomotion and eating behavior changes in Yucatan minipigs after unilateral radio-induced ablation of the caudate nucleus. *Sci Rep*. 2019;9(1):17082. https://doi.org/10.1038/s41598-019-53518-2
62. Cahoon P, Giacometti V, Casey F, et al. Investigating spatial fractionation and radiation induced bystander effects: a mathematical modelling approach. *Phys Med Biol*. 2021;66:225007. https://doi.org/10.1088/1361-6560/ac3119. Epub ahead of print. PMID: 34666318.

How to cite this article: Keshmiri S, Brocard S, Serduc R, et al. A high-resolution dose calculation engine for X-ray microbeams radiation therapy. *Med Phys.* 2022;49:3999–4017. https://doi.org/10.1002/mp.15637